Reac Kinet Mech Cat (2017) 121:225–240
DOI 10.1007/s11144-017-1141-y

Activating effect of cerium in hydrotalcite derived Cu–Mg–Al catalysts for selective ammonia oxidation and the selective reduction of NO with ammonia

Sylwia Basąg[1] · Klaudia Kocoł[1] · Zofia Piwowarska[1] · Małgorzata Rutkowska[1] · Rafał Baran[2] · Lucjan Chmielarz[1]

Received: 24 November 2016 / Accepted: 7 January 2017 / Published online: 20 January 2017

Abstract Hydrotalcite originated mixed metal Cu–Mg–Al oxide system was doped with various amounts of cerium (0.5 or 3.0 wt%) and tested in the role of catalysts for the selective catalytic oxidation of ammonia to dinitrogen (NH_3-SCO) and the selective catalytic reduction of NO with ammonia (NH_3-SCR). The activating effect of cerium was observed in both studied processes. However, the CeO_2 loading is a very important parameter determining catalytic performance of the studied samples. It was shown that an introduction of cerium into Cu–Mg–Al mixed oxide resulted in its significant activation in the low-temperature NH_3-SCR process, independently of the CeO_2 loading and a decrease in the efficiency of the NO reduction at higher temperatures, which was more significant for the catalyst with the lower cerium content. In the case of the NH_3-SCO process, the introduction of cerium into Cu–Mg–Al mixed oxide resulted in the activation of the low temperature reaction, which was more intensive for the catalyst with lower cerium content. These effects were related to the presence of cerium in the form of crystallites of various size and therefore their different reducibility.

Keywords Hydrotalcite · Copper · Cerium · DeNOx · Selective ammonia oxidation

✉ Lucjan Chmielarz
chmielar@chemia.uj.edu.pl

[1] Faculty of Chemistry, Jagiellonian University, Ingardena 3, 30-060 Kraków, Poland

[2] Faculty of Energy and Fuels, AGH University of Science and Technology, Mickiewicza 30, 30-059 Kraków, Poland

Introduction

Nitrogen containing pollutants, such as nitrogen oxides and ammonia, belong to the most serious environmental problems. Nitrogen oxides, mainly NO and NO_2, are produced as the side products of fuel combustion processes as well as in the chemical industry (e.g. N_2O is a side product in nitrogen fertilizer industry). On the other hand, the majority of ammonia emission is related to agricultural activities (e.g. volatilization from livestock wastes, losses from agriculture crops) and additionally to industrial processes and biomass burning [1]. Moreover, increasing ammonia emission is expected in the transportation sector due to the common use of cars with the systems of flue gases purification (e.g. Adblue system in diesel cars and TWC in cars with spark-ignition engines) [2].

The most promising methods for the elimination of nitrogen oxides and ammonia from flue gases are based on their catalytic conversion to the non-toxic products. The NO and NO_2 emitted from stationary and mobile sources are selectively catalytically reduced with ammonia to dinitrogen (NH_3-SCR, $DeNO_x$) [3, 4]. On the other hand, the technology based on the selective catalytic oxidation of ammonia to dinitrogen (NH_3-SCO) has been reported to be the most promising for the elimination of NH_3 from oxygen containing flue gases [1].

Among various catalytic systems studied in the processes mentioned above, the hydrotalcite originated mixed metal oxides containing various transition metals seem to be very promising [5–7]. Hydrotalcites, also called layered double hydroxides (LDHs), are minerals characterized by the brucite-like network, $Mg(OH)_2$, where octahedra of Mg^{2+} are six-coordinated to OH^-. Part of Mg^{2+} cations is substituted by trivalent aluminum cations, what results in the positive charging of the brucite-like layers compensating by anions (typically CO_3^{2-}), which, together with the water molecules, are located in the interlayer space of hydrotalcite. It is possible to synthesize materials with the hydrotalcite structure relatively easily under laboratory conditions. In such hydrotalcite-like materials, Mg^{2+} as well as Al^{3+} ions can be partially or completely replaced by various di- (e.g. Cu^{2+}, Co^{2+}, Ni^{2+}, Zn^{2+}) and/or trivalent (e.g. Fe^{3+}, Cr^{3+}) cations [8]. The range of various metal cations that can be incorporated into the brucite-like layers is relatively broad and is determined by their size, which should be similar to that of Mg^{2+} in the case of divalent cations and to Al^{3+} in the case of trivalent cations [8]. Thermal decomposition of hydrotalcite-like materials results in the formation of mixed metal oxides, which due to their relatively high surface area, porosity and homogenous distribution of metal cations are very promising for potential applications in catalysis [9–11], including also the processes of selective catalytic reduction of NO with ammonia—$DeNO_x$, NH_3-SCR [12, 13] as well as selective catalytic oxidation of ammonia to dinitrogen—NH_3-SCO [1, 5–7].

Our previous studies have shown that the modification of the hydrotalcite originated Cu–Mg–Al mixed oxide with noble metals (Pt, Pd, Rh) resulted in its significant activation in the low-temperature NH_3-SCO process [14]. This effect was explained by the activation of oxygen by noble metals for the reaction of ammonia oxidation. Moreover, it was shown that the process of the selective ammonia

oxidation proceeds in the presence of the hydrotalcite-based catalysts according to the so called internal selective catalytic reduction (i-SCR) [1, 14]. Because of the relatively high cost of noble metals, a cheaper additive, cerium, known to be active in oxygen activation [15, 16], was tested in the frame of the presented studies.

Experimental

Catalyst preparation

The hydrotalcite-like sample with the intended Cu/Mg/Al molar ratio of 5/62/33 was synthesized by a co-precipitation method using aqueous solutions of the following metal nitrates: $Mg(NO_3)_2{\cdot}6H_2O$ (Sigma), $Al(NO_3)_3{\cdot}9H_2O$ (Sigma) and $Cu(NO_3)_2{\cdot}3H_2O$ (Sigma). A solution of NaOH (POCh) was used as a precipitating agent. The solutions of nitrates and NaOH were simultaneously added to a vigorously stirred solution containing Na_2CO_3 (POCh). The pH was maintained constant at 10.0 ± 0.2 by the dropwise addition of NaOH solution. The obtained slurry was stirred at 60 °C for a further 120 min, filtered, washed with distilled water and dried. Finally, the sample was calcined in an air atmosphere at 600 °C for 12 h and then was kept in a desiccator in order to avoid the possible reconstruction of the hydrotalcite structure. The obtained sample is labelled as $Cu_5Mg_{62}Al_{33}$.

The $Cu_5Mg_{62}Al_{33}$ catalyst was doped with cerium by the wet impregnation method using an aqueous solution of $Ce(NO_3)_3{\cdot}6H_2O$. After impregnation, the samples were dried and calcined in an air atmosphere at 600 °C for 12 h. The catalysts doped with 0.5 and 3.0 wt% of cerium are labelled as $Cu_5Mg_{62}Al_{33}$-Ce0.5% and $Cu_5Mg_{62}Al_{33}$-Ce3.0%, respectively.

Characterization of the catalysts

The thermal decomposition of the hydrotalcite-like samples was studied using thermogravimetry coupled with QMS analysis of evolved gases and in situ high temperature XRD. The TGA-DTG-QMS measurements were carried out using a Mettler Toledo 851^e operated under a flow of synthetic air (80 mL min^{-1}) in the temperature range of 25–1000 °C with a linear heating rate of 10 °C min^{-1}. The gases evolved during the thermal decomposition process were continuously monitored by the quadrupole mass spectrometer ThermoStar (Balzers) connected on-line to the microbalance. In-situ high temperature XRD (HT-XRD) measurements were carried out at 25 °C and then from 100 to 900 °C with steps of 100 °C in air using a PANalytical-Empyrean diffractometer (Cu $K_{\alpha 1/2}$ radiation, $\lambda = 1.54060$ Å). Measurements were performed with a sequential temperature increase of 5 °C min^{-1} and with no temperature holding time before each analysis.

The structure and phase composition of the calcined samples were studied by XRD method. The X-ray diffraction patterns of the as-synthesized and calcined samples were recorded in the range of 8°–80° 2θ with steps of 0.02° 2θ by a D2 Phaser diffractometer (Bruker) using Cu $K_{\alpha 1}$ radiation ($\lambda = 1.54060$ Å).

The chemical composition of the calcined hydrotalcite-like samples (cationic ratio) was determined by an electron microprobe analysis performed on a JEOL JCXA 733 Superprobe (electron probe microanalysis, EPMA).

The specific surface area of the calcined samples was determined by N_2 adsorption at −196 °C using a 3Flex (Micromeritics) automated gas adsorption system. Prior to the analysis, the samples were outgassed under vacuum at 350 °C for 24 h. The specific surface area was determined using the BET equation. The total volume of pores (at $p/p_0 = 0.98$) was calculated using the single point model.

The reducibility of the calcined samples was studied by temperature-programmed reduction method (H_2-TPR). Experiments were carried out in a fixed-bed flow microreactor system starting from room temperature to 1000 °C, with a linear heating rate of 5 °C min^{-1}. H_2-TPR runs were carried out in a flow (10 mL min^{-1}) of 5 vol% H_2 diluted in Ar (N5 quality, Messer). The evolution of hydrogen was detected by micro volume TCD (Valco). Prior to the H_2-TPR runs, the samples were outgassed in a flow of pure helium (20 mL min^{-1}) at 600 °C for 1 h.

The DR UV–Vis spectra were recorded using an Evolution 600 (Thermo) spectrophotometer. The measurements were performed in the range of 190–900 nm with a resolution of 2 nm.

Catalytic studies

The calcined samples were tested as catalysts for the selective oxidation of ammonia to nitrogen and water vapor (HN_3-SCO) and for selective catalytic reduction of NO with ammonia ($DeNO_x$, NH_3-SCR). Catalytic tests were done in a fixed-bed flow microreactor system. The analysis of the reaction products was performed using QMS detector (PREVAC). Prior to the activity tests, the sample of the catalyst (200 mg) was outgassed at 600 °C for 1 h in a flow of pure helium (20 mL min^{-1}). The SCO-NH_3 tests were performed in a flow of the reaction mixture containing: $[NH_3] = 0.5$ vol%, $[O_2] = 2.5$ vol% [He] = 97 vol%. The studies were performed in the temperature range of 100–500 °C with a linear heating rate of 10 °C min^{-1}. The $DeNO_x$ tests were carried out in a flow of $[NO] = 0.25$ vol%, $[NH_3] = 0.25$ vol%, $[O_2] = 2.5$ vol% and [He] = 97 vol% in the temperature range of 100–375 °C with a linear heating rate of 10 °C min^{-1}. For both reactions, the total flow rate of the reaction mixture was 40 mL min^{-1}.

Moreover, the reaction of NO oxidation to NO_2 by O_2 was studied by temperature-programmed reaction method. The experiments were carried out with the catalyst sample of 200 mg in a fixed-bed flow microreactor system starting from 100 to 600 °C, with a linear heating rate of 10 °C min^{-1} in a flow of the reaction mixture containing: $[NO] = 0.5$ vol%, $[O_2] = 2.5$ vol% and [He] = 97 vol%. The total flow rate of the reaction mixture was 40 mL min^{-1}. The analysis of the reaction products was performed using QMS detector (PREVAC). Prior to the experiments the samples were outgassed in a flow of pure helium (20 mL min^{-1}) at 600 °C for 1 h.

Results and discussion

The structure of the hydrotalcite-like sample as well as the transformations of its structure occurring during thermal treatment was analyzed by in situ high temperature XRD measurements and thermogravimetric method coupled with QMS analysis of evolved gases. The results of HT-XRD studies are presented in Fig. 1. It can be seen that the diffractogram recorded at 25 °C for the dried sample is typical of the hydrotalcite structure without any reflections of the other phases [8]. Cell parameters of *a* and *c* are 0.31 and 2.31 nm, respectively, while the average crystallite size is about 75 nm. The hydrotalcite structure was not damaged after heating the sample to 100 °C. The *c* parameter after heating the sample to 100 °C was not changed indicating that water molecules located in the interlayer space of the hydrotalcite-like materials was not removed within this temperature range. An increase in temperature from 100 to 200 °C significantly reduced the *c* parameter from 2.31 to 2.07 nm. Thus, it could be concluded that water molecules were intensively evacuated form the interlayer space of the sample in this temperature range. A further increase in temperature to 300 °C resulted in a gradual decrease and broadening of the reflections characteristic of the hydrotalcite structure, which is related to the decreasing long distance ordering of the brucite-like layers and their gradual degradation. At higher temperatures, broad reflections at 2θ values about 35°, 43° and 64°, characteristic of MgO (periclase), were formed. The intensity of these reflections increased with an increase in temperature, which is related to the progressive growth of this crystalline phase. At 900 °C, new reflections at 19°, 31°, 36°, 45°, 59°, 65° and 78° related to the spinel phases (possibly $MgAl_2O_4$ and

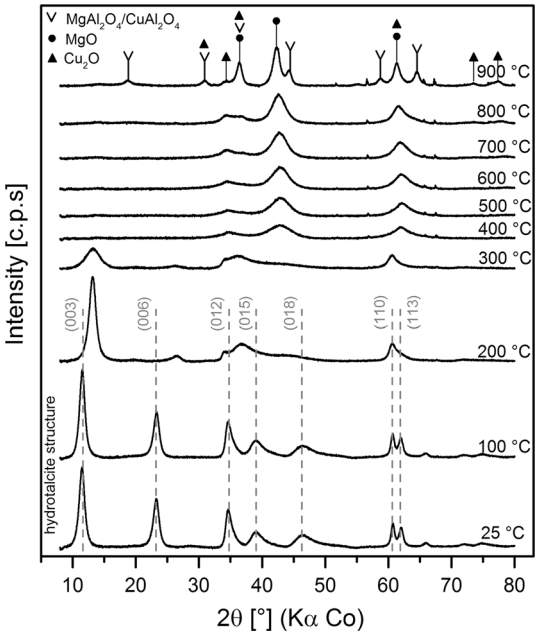

Fig. 1 Results of in situ high temperature XRD measurements for not doped sample. sample: $Cu_5Mg_{62}Al_{33}$. Periclase (● – MgO), cuprite (▲ – Cu_2O) and spinel phases (v - $MgAl_2O_4$ and $CuAl_2O_4$)

$CuAl_2O_4$) appeared in diffractograms [5, 17]. Moreover, the reflections at 31°, 36°, 61°, 73° and 78° could be possibly assigned to cuprite (Cu_2O) [18]. However, it should be noted that the reflections at 31°, 36°, 78° are probably superpositions of the reflections characteristic of Cu_2O and spinel phases, while the reflection at 61° is possibly a superposition of the reflections characteristic of Cu_2O and MgO. Thus, only the weak and broad reflection located at 73° could individually represent the Cu_2O phase and therefore the presence of cuprite in the sample cannot be fully confirmed by in situ XRD studies.

Thermogravimetry coupled with the QMS (quadrupole mass spectrometry) analysis of the released gases (TG-QMS) was another technique used in the studies of thermal deposition of the hydrotalcite-like materials into mixed metal oxides. The results of these studies are presented in Fig. 2. The thermal behavior of hydrotalcites is generally characterized by two main transitions: (i) the first one is related to the loss of interlayer water without collapse of the hydrotalcite structure at relatively low temperatures, while (ii) the second one is associated with the elimination of hydroxyl groups from the brucite-like layers and the decomposition of interlayer

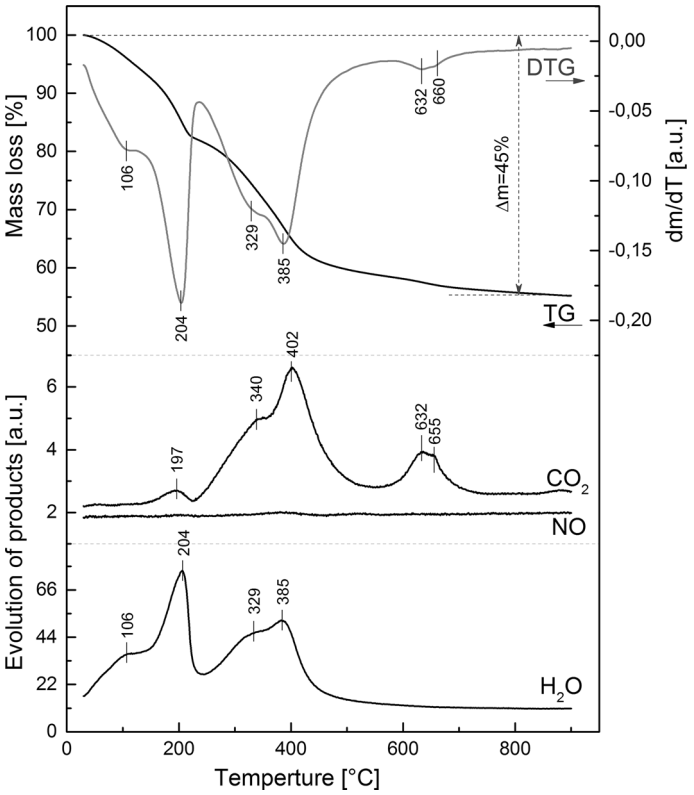

Fig. 2 Results of TG-QMS analysis of the released gases obtained for the not doped $Cu_5Mg_{62}Al_{33}$ sample

anions at higher temperatures [8]. The temperature ranges of these two transitions depend mainly on the composition of the hydrotalcite-like materials.

The DTG peak related to the release of interlayer water from the $Cu_5Mg_{62}Al_{33}$ sample is spread from room temperature to about 230 °C with two minima located at 106 and 204 °C. The low temperature minimum is possibly related to the water adsorbed on the outer surface of the sample grains or crystallites, while the second one, with a minimum at 204 °C, could be attributed to the release of interlayer water molecules [18]. These results are fully consistent with the HT-XRD studies, which showed that the *c* parameter determined for the $Cu_5Mg_{62}Al_{33}$ sample thermally treated at 25, 100 and 200 °C is 2.32, 2.31 and 2.07 nm.

The second stage of the hydrotalcite-like samples decomposition, including dehydroxylation of the brucite-like layers as well as decomposition of interlayer anions, is represented by the DTG peaks and maxima of H_2O and CO_2 evolution located in the range of 230–500 °C. The release of CO_2 and H_2O from the studied sample is represented in this temperature range by double maxima at about 335–350 °C and 385–405 °C. Thus, the OH^- anions in the brucite-like layers as well as interlayer carbonates are differently stabilized in the studied sample. The comparison of the locations for these peaks with temperatures of pure $Al(OH)_3$ and $Mg(OH)_2$ dehydroxylation, which was reported to be about 300 °C [19] and 380 °C [20], respectively, may suggest that the low-temperature peak could be related to the release of OH^- anions attached to aluminum, while the high-temperature peak to the dehydroxylation of OH^- bounded to Mg^{2+} cations. It should be noted that small amount of CO_2 is released at temperatures about 640 °C. A similar effect of the carbonate stabilization in the copper containing hydrotalcite-like samples was observed in our previous studies [18, 21]. Thus, it seems that the formation of such stable carbonates is characteristic of hydrotalcite-like materials containing copper.

Based on the HT-XRD and TG-QMS studies, it was decided to calcine the hydrotalcite-like sample at 600 °C for 12 h. As it was shown under such conditions of thermal treatment, the hydrotalcite-like sample was thermally decomposed to mixed metal oxide system.

Fig. 3 presents diffractograms recorded for the dried hydrotalcite-like sample and its calcined form (600 °C/12 h) as well as the calcined samples doped with cerium (0.5 and 3.0 wt%). The diffractogram recorded for the calcined $Cu_5Mg_{62}Al_{33}$ sample contains the reflections characteristic of periclase (MgO) at 2θ values of 36°, 43° and 64°. The deposition of cerium resulted in an appearance of the reflection characteristic of CeO_2 at about 29°, 47° and 56°. It should be noted that these reflections are present in the samples with as low cerium content as 3 wt%, which could be explained by the tendency of cerium to the formation of aggregated crystallites on the surface of the calcined hydrotalcite sample. In the case of the $Cu_5Mg_{62}Al_{33}$-Ce3.0% sample, the average size of CeO_2 crystallites, determined using the Scherrer method, is about 2.9 nm. The reflections characteristic of CeO_2 in diffractogram recorded for $Cu_5Mg_{62}Al_{33}$-Ce0.5% are characterized by very low intensity, and therefore the determination of the average size of CeO_2 crystallites in this case is impossible. However, the size of CeO_2 crystallites in the $Cu_5Mg_{62}Al_{33}$-Ce0.5% sample is significantly lower in comparison the size of crystallites in $Cu_5Mg_{62}Al_{33}$-Ce3.0%.

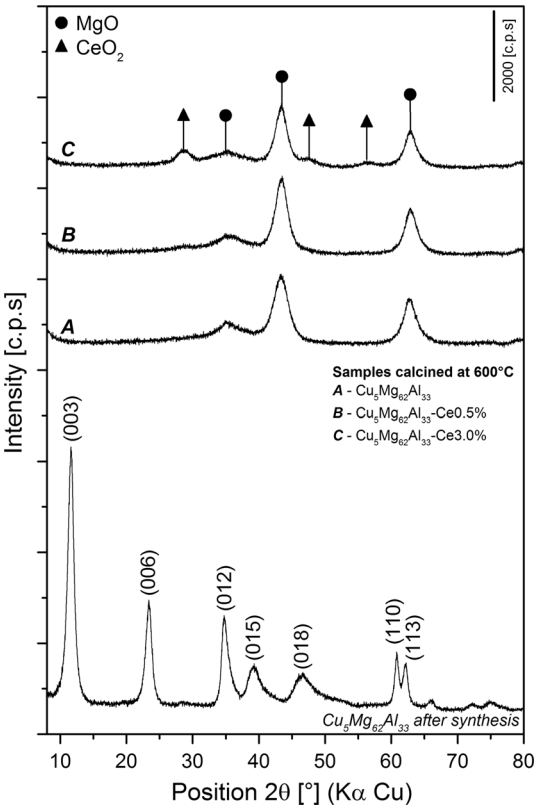

Fig. 3 X-ray diffractograms of not doped sample: $Cu_5Mg_{62}Al_{33}$ dried and calcined at 600 °C and doped with cerium (0.5 and 3.0 wt%). Periclase (*black circle*—MgO) and cerium(IV) oxide (*black triangle*—CeO_2)

The chemical composition and specific surface area of the calcined hydrotalcite-like samples are presented in Table 1. The determined cation ratios in the studied samples are very close to the intended theoretical values. In the case of the studied samples, very similar values of specific BET surface areas of about 240 $m^2\ g^{-1}$ were determined.

The form and aggregation of copper in the $Cu_5Mg_{62}Al_{33}$ sample and its modifications with cerium were studied by UV–Vis-DR spectroscopy (Fig. 4). The spectra recorded for all the studied samples consist of the intensive asymmetric band, which is a superposition of the peaks indicating the charge-transfer between mononuclear Cu^{2+} ion and oxygen as well as copper in the form of oligomeric

Table 1 Chemical composition and specific surface area of calcined hydrotalcite like materials

Sample	Cu/Mg/Al/Ce molar ratio (%)	BET surface area ($m^2\ g^{-1}$)
$Cu_5Mg_{62}Al_{33}$	5.09/59.81/35.1/0.00	239
$Cu_5Mg_{62}Al_{33}$-Ce0.5%	5.03/59.76/35.05/0.16	240
$Cu_5Mg_{62}Al_{33}$-Ce3.0%	5.00/59.38/34.72/0.85	242

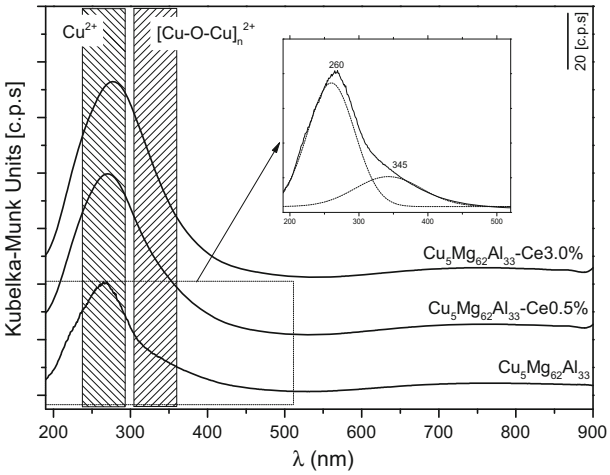

Fig. 4 UV–Vis-DR spectra of the $Cu_5Mg_{77}Al_{18}$ not doped sample and doped with cerium (0.5 and 3.0 wt%) calcined at 600 °C

$(Cu^{2+}–O^{2-}–Cu^{2+})_n^{2+}$ species [22–24]. Moreover, a very broad band centered at about 745–790 nm, is attributed to the d–d transition in Cu^{2+} located in a distorted octahedral coordination [25, 26]. The insert in Fig. 4 presents the result of deconvolution of the original spectrum recorded the $Cu_5Mg_{62}Al_{33}$ sample in the range characteristic of mononuclear and oligomeric copper species. The sharp band centered at about 260 nm is assigned to mononuclear Cu^{2+} ions, while the less intensive peak at about 345 nm is related to the presence of copper in the form of oligomeric copper oxide species. A comparison of the intensity of these bands leads to the conclusion that copper in the form of mononuclear Cu^{2+} cations dispersed in the Mg–Al oxide matrix dominates in the studied sample. Thus, it could be concluded that copper is present in the well dispersed forms in the studied samples: monomeric and small oligomeric species dispersed in the Mg–Al oxide matrix. It should be also noted that introduction of cerium to the calcined hydrotalcite sample did not influence significantly the type and distribution of coppers species.

The reducibility of the hydrotalcite-based catalysts was studied by temperature-programmed reduction (H_2-TPR) method (Fig. 5). The only peak in the H_2-TPR profile of the $Cu_5Mg_{62}Al_{33}$ sample centered at about 230 °C is related to the reduction of Cu^{2+} to Cu^0 [18, 27]. The introduction of cerium to the $Cu_5Mg_{62}Al_{33}$ sample resulted in a shift of this peak into higher temperatures by about 8–10 °C and the appearance of two additional peaks. The first one located at about 110 °C is possibly attributed to the reduction of surface Ce^{4+} to Ce^{3+} by atomic hydrogen species [28, 29]. Such species are formed by the dissociation of the H_2 molecules on the copper surface and then are spilled over to reduce the ceria surface oxygen [29]. The second peak located at 740 and 790 °C for the samples doped with 0.5 and 3.0 wt% of cerium is related to the reduction of Ce^{4+} to Ce^{3+} in CeO_2 [29]. A comparison of the peak intensities and positions leads to the conclusions that there is only a small contribution of surface cerium reduced at low temperatures by atomic

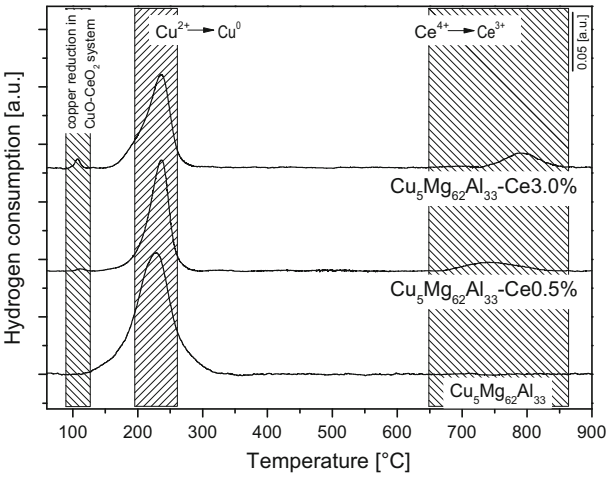

Fig. 5 Results of H_2-TPR analysis obtained for $Cu_5Mg_{62}Al_{33}$ both not doped and doped with cerium (0.5 and 3.0 wt%) calcined at 600 °C

hydrogen formed by the dissociation of H_2 molecules on the copper species and moreover, the reduction of CeO_2 (occurring at higher temperatures) strongly depends on its crystallinity.

The Ce^{3+}/Ce^{4+} ratios in the studied catalysts were determined based on the results of chemical analysis (EPMA, Table 1) and H_2-TPR studies. It was estimated that the molar Ce^{3+}/Ce^{4+} ratios are about 0.08 and 0.31 in the $Cu_5Mg_{62}Al_{33}$-Ce0.5% and $Cu_5Mg_{62}Al_{33}$-Ce3.0% samples.

The $Cu_5Mg_{62}Al_{33}$ sample and its modifications with cerium were tested in the role of the catalysts for the selective catalytic reduction of NO with ammonia (NH_3-SCR, $DeNO_x$) and the selective catalytic oxidation of ammonia (NH_3-SCO).

In the case of the $DeNO_x$ process, dinitrogen is a desired reaction product, while N_2O is an undesired side product. The results of the catalytic studies of this process are presented in Fig. 6. The NO reduction by ammonia in the presence of the $Cu_5Mg_{62}Al_{33}$ catalyst started at about 125 °C and gradually increased to 92% at 325 °C. Above this temperature, the efficiency of the $DeNO_x$ process decreased due to the side process of direct ammonia oxidation by oxygen present in the reaction mixture. It should be noted that the selectivity to dinitrogen in the whole studied temperature range is very high (above 90%). The introduction of cerium to the $Cu_5Mg_{62}Al_{33}$ sample resulted in its significant activation in the low-temperature $DeNO_x$ process. In the case of the $Cu_5Mg_{62}Al_{33}$-Ce05% and $Cu_5Mg_{62}Al_{33}$-Ce3.0% catalysts, the NO conversion profiles were shifted in the direction of lower temperatures by about 30–50 °C in comparison with the $Cu_5Mg_{62}Al_{33}$ sample. This effect was practically independent of the content of introduced cerium. The maximum of the NO conversion on the level of 96% was obtained for both cerium modified catalysts at about 275 °C. Above this temperature, a significant decrease in the efficiency of the NO conversion, much more intensive in comparison with the $Cu_5Mg_{62}Al_{33}$ catalyst and related to the side process of direct ammonia oxidation by

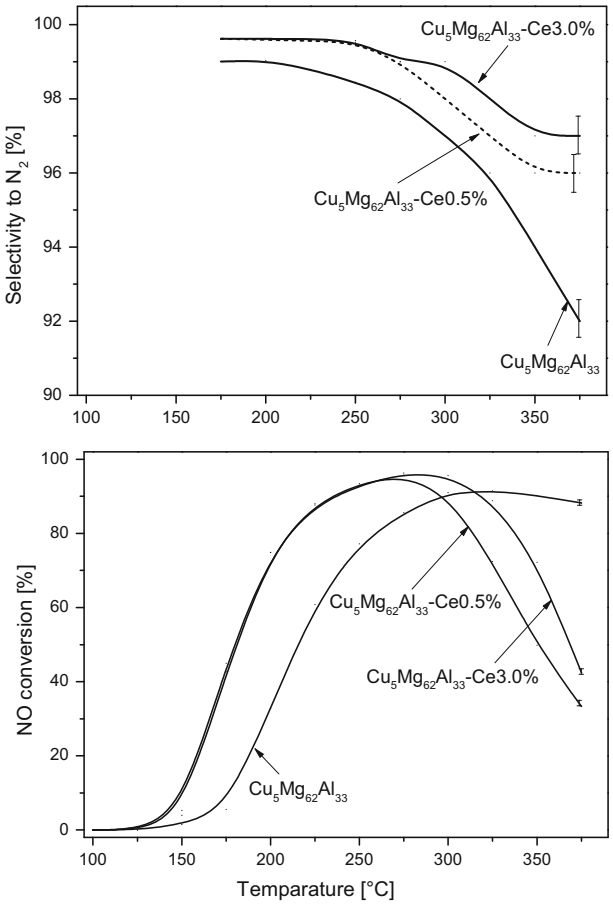

Fig. 6 Results of catalytic tests in the $DeNO_x$ process for the $Cu_5Mg_{62}Al_{33}$ sample not doped and doped with cerium (0.5 and 3.0 wt%) calcined at 600 °C. Experimental error in determination of the NO conversion and selectivity to N_2 is 1% (*error bars* marked in figures)

oxygen, was observed. It should be noted that there are significant differences in the catalytic performances of the samples with various content of cerium in the high temperature range. In the case of the catalyst with lower cerium content ($Cu_5Mg_{62}Al_{33}$-Ce0.5%), a decrease in the efficiency of the NO conversion was significantly more significant in comparison to the sample with higher cerium loading ($Cu_5Mg_{62}Al_{33}$-Ce3.0%). It should also be noted that the selectivity to dinitrogen, obtained in the presence of the cerium doped catalysts, is very high (above 95%) in the whole studied temperature range, including also the high temperature region, where the process of direct ammonia oxidation dominated. Thus, it could be concluded that in this range, ammonia was oxidized nearly exclusively to dinitrogen. The activating role of cerium for the low-temperature $DeNO_x$ process could be explained by supplying reactive oxygen as a result of the Ce^{4+} to Ce^{3+} reduction occurring on the surface of CeO_2 crystallites being in the

contact with copper species (low temperatures) as well as in bulky CeO_2 (high temperatures). As it was shown by H_2-TPR studies (Fig. 5), the size of CeO_2 crystallites is a very important factor influencing the reduction temperature of Ce^{4+} to Ce^{3+}. The Ce^{4+} cations in larger CeO_2 crystallites are significantly more effectively stabilized in comparison with such cations in smaller CeO_2 crystallites. The majority of the mechanisms suggested for the $DeNO_x$ process include ammonia chemisorption and activation as a crucial step [30]. In such mechanisms, oxygen could react with chemisorbed ammonia molecules resulting in proton abstraction and the formation of $–NH_2$ adsorbed species, which could be converted by NO to dinitrogen and water molecules ($–NH_2 + NO \rightarrow N_2 + H_2O$) in the next step. Such a mechanism was suggested in the scientific literature for various catalytic systems [30]. However, it needs verification in the case of the studied catalysts. Active oxygen supplied by CeO_2 could also oxidize NO to very reactive NO_2. The reduction of the mixture of NO and NO_2 with ammonia, known as fast-SCR [31, 32], typically proceeds much more effectively in comparison to the reduction of NO with ammonia. The possible oxidation of NO to NO_2 over the studied catalysts was tested by temperature programmed reaction of NO with oxygen. The results of these studies are presented in Fig. 7. It can be seen that the oxidation of NO to NO_2 occurred for all the studied catalysts. However, in the case of the samples doped with cerium, this effect is more significant. Therefore, it is possible that the activation role of cerium is related to the intensification of the process of NO to NO_2 oxidation. Of course, the activation of the chemisorbed ammonia molecules by cerium cannot be excluded in this stage of the studies. A decrease in the efficiency of the NO_2 formation observed at higher temperatures is due to thermodynamic limitation (the equilibrium profile is presented in Fig. 7). A more intensive decrease in the NO conversion observed for the samples with the lower cerium loading ($Cu_5Mg_{62}Al_{33}$-Ce0.5%) in comparison to the sample with the higher cerium content ($Cu_5Mg_{62}Al_{33}$-Ce3.0%) is possibly related to the higher activity of the smaller CeO_2

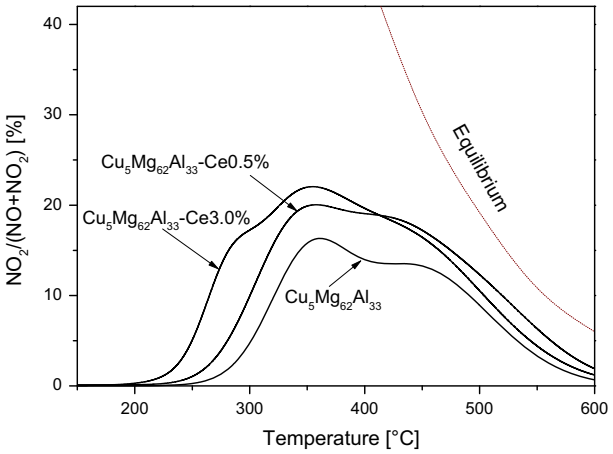

Fig. 7 Results of the oxidation of NO to NO_2 occurred for the $Cu_5Mg_{62}Al_{33}$ not doped and doped with cerium (0.5 and 3.0 wt%) calcined at 600 °C

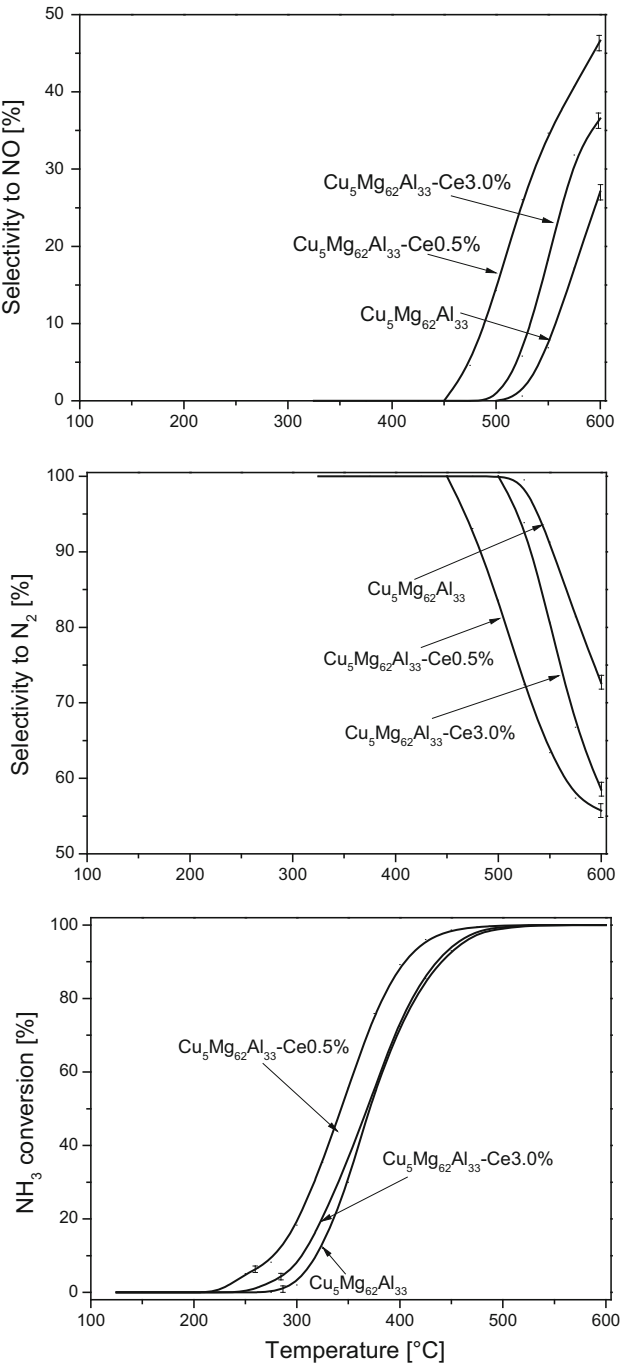

Fig. 8 Results of catalytic tests in the NH_3-SCO process for the $Cu_5Mg_{62}Al_{33}$ not doped and doped with cerium (0.5 and 3.0 wt%) calcined at 600 °C. Experimental errors in determination of the NH_3 conversion and selectivity to NO or N_2 are 1 and 1.5%, respectively (*error bars* marked in figures)

crystallites in the process of direct ammonia oxidation than larger crystalizes of cerium oxide. Taking into account the results of H_2-TPR studies (Fig. 5), this effect is not surprising because the smaller crystallites were reduced ($Ce^{4+} \rightarrow Ce^{3+}$) at significantly lower temperature than larger crystallites of CeO_2.

The second studied process was the selective catalytic oxidation of ammonia (NH_3-SCO) to dinitrogen, which is a desired reaction product. Nitrogen oxides (NO, N_2O and NO_2) are the undesired side products. The results of the catalytic studied of this process are presented in Fig. 8. The NH_3 conversion in the presence of the $Cu_5Mg_{62}Al_{33}$ catalyst started at about 275 °C and continuously increased up to 500 °C, when ammonia was completely converted in the reaction stream. The introduction of a small amount of cerium (0.5 wt%) significantly activated the $Cu_5Mg_{62}Al_{33}$ sample for the low-temperature ammonia oxidation. The ammonia conversion profile of the $Cu_5Mg_{62}Al_{33}$-Ce0.5% catalyst was shifted to lower temperatures by about 25 °C relative to $Cu_5Mg_{62}Al_{33}$. An increase in cerium loading to 3.0 wt% only very slightly increased the ammonia conversion in comparison to the $Cu_5Mg_{62}Al_{33}$ catalyst. Such a significant difference in the activation effect observed for the samples doped with various amounts of cerium is probably, similarly to the $DeNO_x$ process, a result of different stabilization of oxygen in smaller and larger CeO_2 crystallites. The catalyst containing CeO_2 in the form of smaller, and therefore easier reduced ($Ce^{4+} \rightarrow Ce^{3+}$) crystallites was found to be more active in the low temperature range in comparison of the samples with larger crystallites of cerium oxide, which needs higher temperature to reduce Ce^{4+} to Ce^{3+}. N_2 and NO were the main products of ammonia oxidation. Moreover, small amounts of N_2O were formed (not shown in Fig. 8). The formation of any other nitrogen containing products, including NO_2, was not detected. Dinitrogen and water vapor were the only products of ammonia oxidation at temperatures below 450 °C. The formation of NO started in the presence of the most active $Cu_5Mg_{62}Al_{33}$-Ce0.5% catalyst at 450 °C, while in the case of $Cu_5Mg_{62}Al_{33}$ and $Cu_5Mg_{62}Al_{33}$-Ce3.0%, the temperature was about 500 °C. This effect, similarly to the differences in the ammonia conversion, could be explained by various size of CeO_2 crystallites, which can release reactive oxygen at different temperatures. Therefore, in the case of the $Cu_5Mg_{62}Al_{33}$-Ce0.5% sample oxidation of ammonia can be "deeper" and results in the formation of NO at lower temperatures than for $Cu_5Mg_{62}Al_{33}$-Ce3.0%.

Conclusions

The hydrotalcite originated mixed metal Cu–Mg–Al oxide system was found to be effective catalyst for the selective reduction of NO with ammonia ($DeNO_x$, NH_3-SCR) and selective oxidation of ammonia to dinitrogen (NH_3-SCO). The further catalytic activation of such metal oxide system, especially for the low-temperature processes, was possible by the deposition of small amounts of cerium (0.5 or 3.0 wt%) using the impregnation method. It was shown that in the case of the $DeNO_x$ process doping of mixed metal Cu–Mg–Al oxide with cerium resulted in its significant activation in the low-temperature range independently of the cerium

loading. On the other hand, a decrease in the NO conversion, related to the side process of direct ammonia oxidation, was less intensive for the sample with higher cerium loading. In the case of the NH_3-SCO process, only doping of the calcined hydrotalcite with a small amount of cerium (0.5 wt%) resulted in a significant activation of the catalyst for the low-temperature process. These differences in the catalytic properties of the samples loaded with various amounts of cerium were explained by the different size of deposited CeO_2 crystallites. It was shown that the reduction of Ce^{4+} to Ce^{3+} occurs in smaller CeO_2 crystallites at temperatures significantly lower in comparison with the larger crystallites of cerium oxide. It seems that the redox properties of the catalysts are crucial for their performance in the studied processes.

References

1. Chmielarz L, Jabłońska M (2015) Advances in selective catalytic oxidation of ammonia to dinitrogen: a review. RSC Adv 54:43408–43431
2. Zhao D, Wang A (1994) Estimation of anthropogenic ammonia emissions in Asia. Atmos Environ 28:689–694
3. Li J, Chang H, Ma L, Hao J, Yang RT (2011) Low-temperature selective catalytic reduction of NO_x with NH_3 over metal oxide and zeolite catalysts—a review. Catal Today 25:147–156
4. Yadav D, Prasad R (2016) Low temperature de-NO_x technology—a challenge for vehicular exhaust and its remedation: an overview. Proc Tech 24:639–644
5. Jabłońska M, Chmielarz L, Węgrzyn A, Guzik K, Piwowarska Z, Witkowski S, Walton RI, Dunne PW, Kovanda F (2013) Thermal transformations of Cu-Mg(Zn)–Al(Fe) hydrotalcite-like materials into metal oxide systems and their catalytic activity in selective oxidation of ammonia to dinitrogen. J Therm Anal Calorim 114:731–747
6. Chmielarz L, Kuśtrowski P, Rafalska-Łasocha A, Dziembaj R (2005) Selective oxidation of ammonia to nitrogen on transition metal containing mixed metal oxides. Appl Catal B Environ 58:235–244
7. Chmielarz L, Węgrzyn A, Wojciechowska M, Witkowski S, Michalik M (2011) Selective catalytic oxidation (SCO) of ammonia to nitrogen over hydrotalcite originated Mg–Cu–Fe mixed metal oxides. Catal Lett 141:1345–1354
8. Cavani F, Trifiro F, Vaccari A (1991) Hydrotalcite-type anionic clays: preparation, properties and applications. Catal Today 11:173–301
9. Nishida K, Li D, Zhan Y, Shishido T, Oumi Y, Sano T, Takehira K (2009) Effective MgO surface doping of Cu/Zn/Al oxides as water-gas shift catalysts. Appl Clay Sci 44:211–217
10. Xu S, Liao MC, Zeng HY, Chen CR, Duan HZ, Liu XJ, Du JZ (2015) Magnetic hydrotalcites as solid basic catalysts for cellulose hydrolysis. Appl Clay Sci 115:124–131
11. Zhang LH, Li F, Evans DG, Duan X (2010) Cu–Zn-(Mn)–(Fe)–Al layered double hydroxides and their mixed metal oxides: physicochemical and catalytic properties in wet hydrogen peroxide oxidation of phenol. Ind Eng Chem Res 49:5959–5968
12. Chmielarz L, Kuśtrowski P, Rafalska-Łasocha A, Majda D, Dziembaj R (2002) Catalytic activity of Co–Mg–Al, Cu–Mg–Al and Cu–Co–Mg–Al mixed oxides derived from hydrotalcites in SCR of NO with ammonia. Appl Catal B Environ 35:195–210
13. Wang Z, Li Q, Wang L, Shangguan W (2012) Simultaneous catalytic removal of NO_x and soot particulates over CuMgAl hydrotalcites derived mixed metal oxides. Appl Clay Sci 55:125–130

14. Chmielarz L, Jabłońska M, Strumiński A, Piwowarska Z, Węgrzyn A, Witkowski S, Michalik M (2013) Selective catalytic oxidation of ammonia to nitrogen over Mg–Al, Cu–Mg–Al and Fe–Mg–Al mixed metal oxides doped with noble metals. Appl Catal B 130–131:152–162
15. Good J, Duchesne PN, Zhang P, Koshut W, Zhou M, Jin R (2017) On the functional role of the cerium oxide support in the$Au_{38}(SR)_{24}/CeO_2$ catalyst for CO oxidation. Catal Today 280:239–245
16. Jeirani Z, Soltan J (2016) Ozonation of oxalic acid with an effective catalyst based on mesoporous MCM-41 supported manganese and cerium oxides. J Water Proc Eng 12:127–134
17. Kannan S, Rivers V, Knözinger H (2004) High-temperature transformations of Cu-rich hydrotalcites. J Solid State Chem 177:319–331
18. Basąg S, Piwowarska Z, Kowalczyk A, Węgrzyn A, Baran R, Gil B, Michalik M, Chmielarz L (2016) Cu–Mg–Al hydrotalcite-like materials as precursors of effective catalysts for selective oxidation of ammonia to dinitrogen—the influence of Mg/Al ratio and calcination temperature. Appl Clay Sci 129:122–130
19. Taguchi M, Nakane T, Hashi K, Ohki S, Shimizu T, Sakka Y, Matsushit A, Abe H, Funazukuri T, Naka T (2013) Reaction temperature variations on the crystallographic state of spinel cobalt aluminate. Dalton Trans 42:7167–7176
20. Li Y, Lu G, Ma J (2014) Highly active and stable nano NiO–MgO catalyst encapsulated by silica with a core-shell structure for CO_2 methanation. RSC Adv 4:17420–17428
21. Jabłońska M, Chmielarz L, Węgrzyn A, Góra-Marek K, Piwowarska Z, Witkowski S, Bidzińska E, Kuśtrowski P, Majda D (2015) Hydrotalcite derived (Cu, Mn)–Mg–Al metal oxide systems doped with palladium as catalysts for low-temperature methanol incineration. Appl Clay Sci 114:273–282
22. Marion MC, Garbowski E, Primet M (1990) Physicochemical properties of copper oxide loaded alumina in methane combustion. J Chem Soc Faraday Trans 86:3027–3032
23. Martins L, Peguin RPS, Wallau M, Urquieta González EA (2004) Cu-, Co-, Cu/Ca- and Co/Ca-exchanged ZSM-5 zeolites: activity in the reduction of NO with methane or propane. Stud Surf Sci Catal 154 C:2475–2483
24. Mendes FMT, Schmal M (1997) The cyclohexanol dehydrogenation on Rh-Cu/Al_2O_3 catalysts part 1. Characterization of the catalyst. Appl Catal A 151:393–408
25. Praliaud H, Mikhailenko S, Chajar Z, Primet M (1998) Surface and bulk properties of Cu-ZSM-5 and Cu/Al_2O_3 solids during redox treatments. Correlation with the selective reduction of nitric oxide by hydrocarbons. Appl Catal B 6:359–374
26. Das SK, Mukherjee S, Lopes LMF, Ilharco LM, Ferraria AM, Botelho AM, Pombeiro AJL (2014) Synthesis, characterization and heterogeneous catalytic application of copper integrated mesoporous matrices. Dalton Trans 43:3215–3226
27. Chmielarz L, Piwowarska Z, Rutkowska M, Wojciechowska M, Dudek B, Witkowski S, Michalik M (2012) Total oxidation of selected mono-carbon VOCs over hydrotalcite originated metal oxide catalysts. Catal Commun 5:118–125
28. Zheng XC, Zhang XL, Wang XY, Wangand SR, Wu SH (2005) Preparation and characterization of CuO/CeO_2 catalysts and their applications in low-temperature CO oxidation. Appl Catal A 295:142–149
29. Beckers J, Rothenberg G (2008) Redox properties of doped and supported copper–ceria catalysts. Dalton Trans 46:6573–6578
30. Busca G, Lietti L, Ramis G, Berti F (1998) Chemical and mechanistic aspects of the selective catalytic reduction of NO_x by ammonia over oxide catalysts: a review. Appl Catal B 18:1–36
31. Pérez Vélez R, Ellmers I, Huang H, Bentrup U, Schünemann V, Grünert W, Brückner A (2014) Identifying active sites for fast NH_3-SCR of NO/NO_2 mixtures over Fe-ZSM-5 by operando EPR and UV–Vis spectroscopy. J Catal 316:103–111
32. Iwasaki M, Shinjoh H (2010) A comparative study of "standard", "fast" and "NO_2" SCR reactions over Fe/zeolite catalyst. Appl Catal A 390:71–77